MODELLING ICE Ic OF DIFFERENT ORIGIN AND STACKING-FAULTED HEXAGONAL ICE USING NEUTRON POWDER DIFFRACTION DATA

T.C. Hansen[1,2], A. Falenty[2] and W.F. Kuhs[2]

[1]Institut Max von Laue-Paul Langevin, BP 156, 38042 Grenoble Cedex 9, France
[2]Geowissenschaftliches Zentrum der Universität Göttingen, Abteilung Kristallographie, Goldschmidtstraße 1, 37077 Göttingen, Germany

1 INTRODUCTION

1.1 Background

1.1.1 Formation of ice Ic. Ice Ic (named cubic ice by König[1]), known as a further solid crystalline phase at ambient pressure since 1943[1], can be obtained only in the form of very small crystallites[1-12]. The formation of bulk ice Ic requires special approaches such as relaxation of recovered high-pressure polymorphs of ice (e.g., II, V, XII, IX, VII, VIII and HDA)[4, 7, 13-15] upon warming at ambient pressure, condensation of water vapour at temperatures from 130 to 150 K[16], hyper-quenching liquid water at 170 to 190 K[2, 3], freezing of pore water[17], or by homogeneous freezing of micrometer sized aqueous droplets[18, 19].

1.1.2 Ice Ic in nature. The shape of snowflakes made crystallographers anticipate that ordinary ice would show a hexagonal symmetry. However, studies of the topology of a snowflake and the ice-crystal growth patterns suggested later[20] that some dendrite snow flakes grow from a nucleus of cubic ice. In the 1980s, Whalley[21] reasoned that water droplets may freeze to cubic ice crystals of substantial size and deduced that the 28° halo around the Sun, which had been first described in Christopher Scheiner's 20 March 1629 notes[22], may have been formed by refraction of light passing through the octahedral crystals of cubic ice in the atmosphere. Further evidence of ice Ic in the atmosphere has been provided more recently[23]. Murray et al.[18, 19] reproduced atmospheric conditions in laboratory experiments and thus confirmed the atmospheric presence of ice Ic when micrometer-sized droplets freeze below 190 K, corresponding to conditions in the polar stratosphere and tropical tropopause. As a metastable phase, ice Ic has a higher vapor pressure than ice Ih, and as a result together with the transformation to ice Ih, ice crystals in clouds at 180 K to 200 K will be larger. These crystals can more efficiently dehydrate air and thus enhance the dehydration of the tropopause[24].

1.1.3 Metastability of ice Ic. Above 150 K ice Ic is unstable with respect to hexagonal ice Ih. The transition takes place over a large temperature range, slowly at 150 K, faster at 190 and 210 K. It depends, again, on the way the cubic ice was produced. Even at these temperatures, the transition is not complete but leaves a stacking faulted hexagonal ice, which transforms further to pure ice Ih above 240 K as shown by an *in situ* neutron powder diffraction study[25] and an *ex situ* X-ray diffraction investigation[18]. Moreover, ice Ic

and defective ice Ih is formed at temperatures well above 200 K upon decomposition of gas hydrates as observed in time-resolved neutron diffraction experiments[25]. It appears that ice Ic is stable up to the melting point if it crystallizes in sufficiently small mesopores (a few nm)[26]. A number of papers discuss the energetic differences of ice Ih/ice Ic in their pure forms, e.g. based on dipole energies[27] or on MD[28].

1.1.4 Diffraction pattern of ice Ic. None of the obtained ice Ic phases show a diffraction pattern corresponding to well-crystallized cubic ice[2, 3, 6-9]. Moreover, the deviations from this idealized structure are different for different starting materials[1-3, 5-11, 17]. The appearance of broad reflections in neutron diffraction experiments with intensities not[19] in agreement with a simple cubic structure was first explained by anisotropic particle size effects[8]. A closer peak shape investigation of the main cubic reflections and the appearance of broad peaks at Bragg angles typical for ice Ih lead to the assignment of the underlying defects as deformation stacking faults[11].

The powder pattern of ice Ic (e.g., Figure 2) shows the reflections 111, 220, 222, 331, 422, 511, 333, 440, 531, 442. Considering isotropic spherical particles, the evaluation of the 111, 220, 222 and 440 peaks according to the Scherrer formula leads to a diameter of 160 Å for ice Ic from ice II.[11] The skewness of the 111 and 222 reflections (shoulder at the high-angle, respectively at the low-angle side) indicate qualitatively the presence of so-called deformation-faults in contrast to so-called growth-faults[29]. The first diffraction peak, best visible in ice Ic samples from ice IX, cannot be indexed with a cubic symmetry and corresponds to the 100 peak of hexagonal ice Ih. It's presence (and the absence of further hexagonal reflections) cannot be explained by a high concentration of growth faults, but with either the existence of thin hexagonal sequences or by the occurrence of regular stacking sequences (polytypes).[11]

Here, a *fault* is defined as a break in the sequence of alternation of close-packed layers. A *growth* fault in a cubic close packed lattice (f.c.c.) is the introduction of one hexagonal packing: ABCABCABCAB becomes ABCAB<u>A</u>**CBACB**, the whole layer sequence is mirrored from the faulty plane onwards. A *deformation* fault corresponds to the formation of two adjacent hexagonal packing sequences: The layer sequence becomes ABCAB<u>AB</u>**CABC**. Starting from a hexagonal close packed lattice (h.c.p.) a *growth* fault corresponds to the formation of one cubic packing sequence: ABABAB becomes AB<u>C</u>**BCB** (structures of 2nd type).[30] A *deformation* fault corresponds to the introduction of two (structures of 3rd type) or three cubic packing sequences (structures of 1st type).[30] In all cases, more complex types of faults can be defined.

1.2 Motivation

To quantify the amount of the resulting ice phase from diffraction data a proper description of these defective ice phases is needed. Here we present a way to fit the diffraction peak profiles with different models of stacking disorder[30]. This may allow us to distinguish different samples with different histories in terms of their stacking distributions. An adapted range of sufficiently large unit cells with different, non-random stacking sequences is created for each sample and a linear combination of these replicas is fitted to the measured neutron diffraction data. In this way a quantitative determination of the total amount of ice present can be obtained.

2 EXPERIMENTAL

2.1 Samples and measurements

The D_2O ice samples investigated in this context were prepared inside vanadium sample cans inside an Orange Cryostat on the constant wavelength neutron powder diffractometers D2B (wavelength 1.6 Å) and D20[31, 32] (wavelength 2.4 Å), based at the high-flux reactor of the Institut Laue-Langevin (ILL). Precursors were high-density amorphous ice (HDA), and the crystalline high-pressure ice phases V and IX, recovered at ambient pressure and 77 K. Ice Ic was obtained by warming the high-pressure phases at ambient pressure. All neutron diffraction data were collected *in situ*.

2.2 Computing

2.2.1 Model generation. First we have to define the basic layer of hexagonal and cubic ice, which will be stacked afterwards following rules for hexagonal or cubic stacking. With the layers as defined subsequently, the terminology of stacking faults as used for close packed metals can be applied correspondingly to ice Ih/Ic. As one layer we shall regard here the two one-fold oxygen atom positions, which lay in a lattice of hexagonal metric (subgroup P3m1 of the space groups $P6_3/mmc$ of ice Ih) on the same fractional *x* and *y* coordinates, but at different *z*. There are three different value pairs (*xy*) possible: (00), (⅓⅔) and (⅔⅓). The fractional heights (*z*) in a hypothetical one-layer cell (half the height of the ice Ih cell in direction of the *c* axis) are – idealized for the purely cubic case – ⅛ and ⅞ respectively. The three different possible layers shall be called A, B and C respectively. Two half-occupied disordered deuterium position is on the bonding lines between two oxygen atoms of same fractional coordinates *x* and *y* in one layer, and two three-fold half occupied ones are between two neighbouring oxygen atoms of adjacent layers. The layers are equivalent but two same layers cannot follow each other. Hexagonal stacking (*h*) occurs when a new layer is similar to the layer preceding the previous one, e.g., (A-)B-A (the hexagonal structure 2H of ice Ih). Cubic stacking (*c*) occurs when the third layer is different from the first one, e.g., A-B-C (the cubic structure 3C of ideal ice Ic). A given stacking sequence, e.g., *hhc*, may be realizable only in a unit cell with a number of layers being a multiple of the periodicity of the stacking sequence (here 3) to fulfil the periodic boundary conditions of a crystal, here (A-B-)A-B-C-B-C-A-C-A-B, the so-called 9R lattice[33] (Figure 1). The stacking variants can thus be equally characterised by the sequence of layers A, B and C or by the sequence of cubic or hexagonal stacking, *c* and *h*.

For stacking sequences of a certain height the number of possible models soon exceeds a number of distinct models, which can be treated one by one, and we have to create models by using probabilities. In the simplest case (s=2), one probability is used to determine if a stacking is cubic or hexagonal (no interactions between two layers). In a more complex case (s=3)[34] two probabilities are used, one (α) to determine, if a cubic stacking follows a hexagonal one, and another (β) to determine, if a cubic stacking follow a cubic one (interaction only with the directly adjacent layer). In the investigation of ice Ic as resulting from relaxation of ice IX it revealed useful to go a step further (s=4)[35] and to work with four probabilities (α, β, γ and δ), determining the probability that a cubic stacking (*c*) follows one of four possible combinations of hexagonal and cubic stacking (*hh*, *hc*, *ch* and *cc*) in the two previous layers. This interaction range is required to obtain, e.g., the 9R lattice, of which the prototype is samarium metal[33]. It was not considered worthwhile to go for an even higher interaction range.

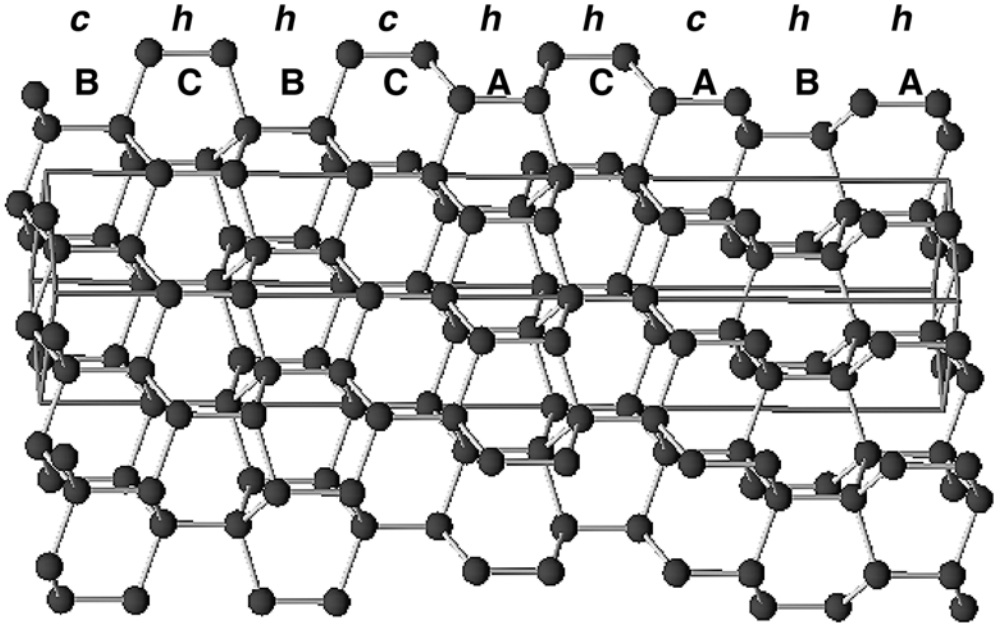

Figure 1 *Structure model of hhc-ice (9R), only the oxygen positions are shown*

Thus, using the programming package Igor[36], a routine was written which, for a given number of layers in a stacking variant of ice Ic/Ih, creates possible stacking sequences based upon the four probabilities for s=2 (or less for s<4). Each new sequence is forwarded either into a routine computing neutron powder diffraction patterns or as a starting model into a Rietveld refinement program (FullProf[37]). Within this, a limited number of parameters (e.g., size and strain peak broadening, scale factor) can be refined to fit the modelled structure to the diffraction data. Instrumental parameters (i.e. the instrument resolution dependent peak widths), peak shape parameters and other parameters related to the sample (size broadening, atomic thermal displacement), were previously refined from a pure ice Ih sample. This sample was measured in exactly the same conditions as it results from the transition of ice Ic to Ih through heating in the same experimental set-up. The resulting figures of merit of a fit to the given powder diffraction data set is stored in a table, together with the effective stacking probabilities for this particular model. The table is kept sorted after a figure of merit, and the probabilities used to create new models are taken from the computed values for the model having given the best fit so far. Once no more new models can be created with the given number of layers (for a low number of layers), or if the number of tries to obtain a new model from the probability-driven, random-generator dependent model generator exceeds a given value, the number of layers is increased by one.

In a first approximation we assume that the displacements of the lattice nodes due to the presence of a stacking "fault" are negligibly small, although there is a small difference of the interlayer distance in ice Ih compared to what one would expect in a purely cubic ice Ic, due to the non-ideal c/a ratio in ice Ih[38]. Note that the term "fault" is ambiguous in the case of cubic ice since it cannot strictly be described as belonging to either the cubic or the hexagonal system. Therefore, one intra-layer oxygen-oxygen distance in ice Ih differs from the three symmetry-equivalent inter-layer oxygen-oxygen distances.

2.2.2 Analytical approach. An alternative to this Monte-Carlo like procedure leading to individual crystalline models fitting only relatively well the observed data, is an analytical description of diffraction patterns based on the stacking fault probabilities and thus on the resulting layer-layer correlation probability distribution, which has been tried for the description of ice in mesopores[26]. Analytical approaches have been widely used for the de-

scription of one-dimensional stacking disorder of close-packed metals since half a century[29]. They have been mostly based on single-crystal diffraction data, allowing for a more detailed and direct observation of the kind of stacking disorder than powder diffraction data would permit. Such an approach has been successfully applied to the structure of lithium metal at different temperatures[35]. However, one deals in that case with low stacking-fault probabilities where a simple classification of faults in twin, growth and deformation faults is appropriate. In this investigation, this approach has not been used, except for getting a qualitative hint of how to interpret the diffraction patterns' particularities, just as it had already been done in the first attempt to explain the defect nature of ice Ic by stacking faults: Kuhs et al.[11] took the indication for deformation faults in a basically cubic ice (double hexagonal stacking ...*chhc*…, in the *s*=4 case, this would correspond to α=1, $\beta\approx1$, γ=0, $\delta\approx1$) from the *hkl*-specific broadening and skewness of higher angle peaks of ice Ic from ice II. Morishige and Uematsu[26] used a related approach to interpret the skewness of the hexagonal 100-peak in ice Ic confined in mesopores as growth faults in a basically hexagonal ice (single cubic stacking …*hhchh*…, in the *s*=4 case, this would correspond to $\alpha\approx0$, β=0, $\gamma\approx0$, δ=0). However, a quantitative full-pattern analysis has not been presented yet.

Inspired by this analytical approach we performed an alternative modelling approach no longer based on a single Monte-Carlo-created single structure model. The later fits reasonably well to the pattern, but does not necessarily represent the average structure very well. With different stacking probabilities α, β, γ and δ (varying each from 0.1 to 0.9 in steps of 0.2) a set of 10 ice supercells of 66 layers have been created. 10 corresponding powder patterns were calculated using Fullprof[39] with instrumental parameters previously refined on an ice Ih reference sample and added together, representing thus a rough general pattern for one of the 5^4 combinations of probabilities (if computing time permits, the steps should be smaller, the supercells larger and the number of individual models higher). One can easily determine the pattern fitting the data best and thus the representative stacking probabilities. The disadvantage of this method is the impossibility at this stage to refine further parameters like the anisotropic size-broadening using a standard Rietveld refinement program such as Fullprof[39].

3 RESULTS

The diffraction patterns of ice Ic from ice V and HDA, measured on D2B, show, compared to ice Ic from ice IX, a relatively weakly expressed 100 Bragg peak of hexagonal ice Ih. A simple modelling with *s*=2 (one simple probability of cubic or hexagonal stacking) delivers a reasonable fit which cannot be distinguished from the case *s*=3 (probabilities for a given stacking depending on previous stacking, thus two probabilities).

The best fitting models for ice Ic as obtained from the relaxation of ice IX revealed some similarity to a 9R lattice combined with large sequences of only cubic stacking. Lower interaction range models (*s*=2 or *s*=3) are not sufficient to model the particularities of the pattern. This alone is already an important qualitative result in itself: Ice Ic formed by the decomposition of ice IX is not just a cubic phase with statistically distributed faults in form of hexagonal stacking sequences, but there are characteristic patterns of how the hexagonal stacking sequences appear in a matrix of cubic stacking. Ice Ic as obtained from decomposition of ice II or HDA has a higher degree of cubic stacking and therefore a lower interaction range (*s*=2) is able to produce models, which are relatively well fitting the observed data.

From D2b data we obtained a structure model through the iterative generation of stacking variants delivering best possible Rietveld fits from a single structural model. The

stacking probabilities for the best fitting models converges slowly to α=0.7, β=0.1, γ=0.1, δ=0.8 which is close to the 9R and the 3C lattice. The ratio of cubic packing versus hexagonal packing converges very clearly to 45% versus 55%. The structure models obtained from D20 data on a different ice Ic sample from recovered ice IX converge to slightly different models with α=0.5, β=0.2, γ=0.2, δ=0.8 with the same ratio of cubic packing of 45%.

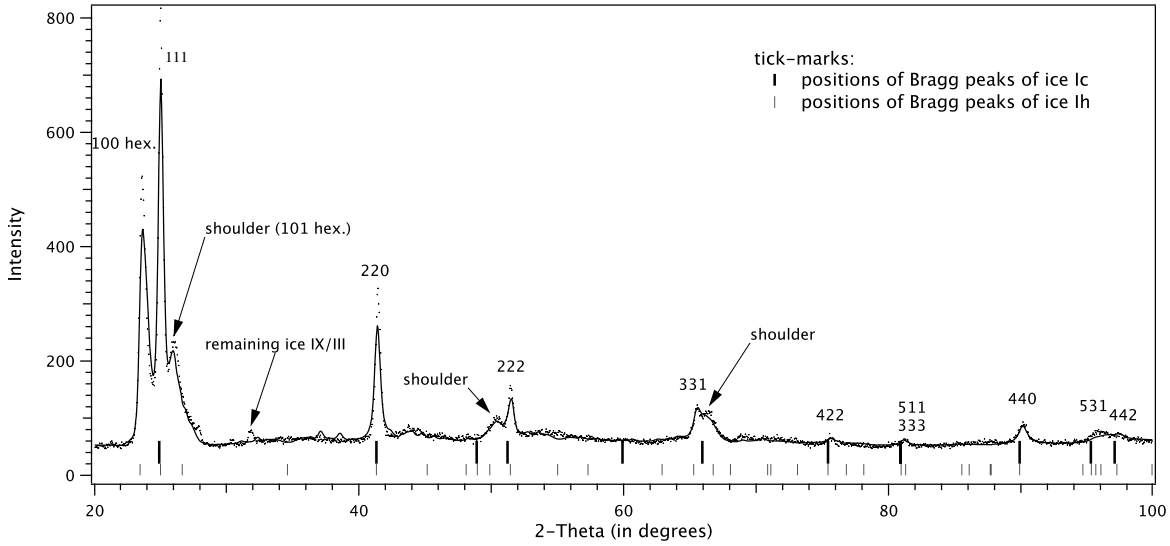

Figure 2 *Diffraction pattern (markers) of ice Ic from ice IX measured at D2b with λ=1.6 Å and Rietveld fit (solid line) of best fitting model; the ticks mark theoretical peak positions for ice Ic (above) and Ih (below), with lattice constants calculated from those of the refined model*

4 DISCUSSION

The drawback of modelling the structure of bulk samples with a complex stacking sequence is that even a structure with 50 layers or more cannot be considered as a unique model to describe the bulk sample. At the given instrumental resolution of the diffractometers there is not visible influence to the diffraction pattern of two layers, which are at a distance of about 100 Å from each other. However, the modelled patterns are far from being as smooth as the measured ones. The structure is thus best modelled by an average of a reasonable number of individual structure models, characterized by the stacking probabilities as given. This could be achieved by a linear combination of patterns from a set of reasonable models and then extracting the stacking probabilities from the result. However, the data do not allow a stable refinement yet. Equivalent to a stacking probability description of the structure, the layer-layer correlation probability can be used as a fingerprint of a given Ic structure.

A second difficulty is the anisotropic size and strain broadening of the diffraction peaks, which is considerable as well, but highly correlated with the broadening due to stacking disorder. A de-convolution is not possible without determining the anisotropic size distribution, e.g., with electron microscopy, which is difficult to perform due to technical temperature and pressure constraints making it impossible to observe a stable sample of ice Ic.

5 CONCLUSIONS

An improved modelling of the average structure of ice Ic includes linear combination of stacking-probability driven structure models and anisotropic size broadening. It allows for a quantitative modelling of neutron diffraction data of different ice Ic samples. It will serve as well for the description of ice Ih samples with stacking faults.

5.1 Outlook

5.1.1 Layer-layer correlation probabilities. The analytical approach described by Berliner and Werner[35] is worth to be pursued further. From the four independent stacking probabilities corresponding to an interaction range of s=4, layer-layer correlation probabilities can be readily computed by a numerical approach[35] for any finite crystallite size. It is then less trivial to compute the precise diffraction pattern corresponding to a correlation probability, and then to refine the parameters – the stacking probabilities – to fit an observed pattern. In principle, even the anisotropic size broadening can be taken into account in this approach as well as deviations from the layer positions.

5.1.2 Small-angle neutron scattering (SANS). Due to the ambiguities of the described modelling of ice Ic one should consider further experiments to distinguish possible scenarios. It is not yet shown, that we deal with a homogeneous sample or with a heterogeneous mixture of two or more phases with a given dispersion around different structure models. Small angle scattering will give helpful hints here as it did in the investigation of HDA[40] Additionally, SANS will reveal the size of suggested blocks of purely cubic stacking and of the 9R-like stacking in ice Ic as obtained from ice IX.

5.1.3 In situ transformation of ice Ic. It is planned to follow in detail the evolution of the stacking probabilities during the slow transformation of ice Ic to ice Ih. It gives a key to the exact process of rearranging the layers and thus to the kinetics observed, which is different for samples of different origin.

5.1.4 Stacking-faulty ice Ih. In this context it is of particular interest to describe the stacking-faulted ice Ih as it results from the decomposition of ice Ic but as well of gas-hydrates below 240 K[25]. It is still not entirely understood why these faults stay stable below 240K. The knowledge of the exact nature of the stacking faults will help to determine the amount of bond-breaking necessary to obtain a stacking fault free sample. This determines the activation energy and thus the transition kinetics at different temperatures.

5.1.5 Reconstructive phase transitions leading to ice Ic. One could gain insight from a quantitative description of the stacking faults in terms of a first or better understanding the reconstructive phase transitions that lead to the formation of different cubic ices, i.e. whilst minimizing the breaking of H-bonds upon restructuring.

Acknowledgements

The presenting author (T.C. Hansen) thanks the University of Göttingen for the opportunity to perform a sabbatical stay including pleasure of teaching crystal chemistry during the long shutdown of the ILL's high-flux reactor for major upgrading.

References

1 H. König, *Z. Krist.*, 1943, **105**, 279.
2 E. Mayer and A. Hallbrucker, *Nature*, 1987, **325**, 601.
3 I. Kohl, E. Mayer, and A. Hallbrucker, *Phys. Chem. Chem. Phys.*, 2000, **2**, 1579.
4 E. F. Burton and W. F. Oliver, *Proc. R. Soc. London, A*, 1935, **153**, 166.

5 N. D. Lisgarten and M. Blackman, *Nature*, 1956, **178**, 39.
6 F. V. Shallcross and G. B. Carpenter, *J. Chem. Phys.*, 1957, **26**, 782.
7 L. G. Dowell and A. P. Rinfret, *Nature*, 1960, **188**, 1144.
8 G. P. Arnold, E. D. Finch, S. W. Rabideau, and R. G. Wenzel, *J. Phys.*, 1968, **49**, 4354.
9 A. Elarby-Aouizerat, J. F. Jal, J. Dupuy, H. Schildberg, and P. Chieux, *J. Phys. C1*, 1987, **48**, 465.
10 J. E. Bertie and S. M. Jacobs, *J. Chem. Phys.*, 1977, **67**, 2445.
11 W. F. Kuhs, D. V. Bliss, and J. L. Finney, *J. Phys. C1*, 1987, **48**, 631.
12 J. Huang and L. S. Bartell, *J. Phys. Chem.*, 1995, **99**, 3924.
13 J. E. Bertie, L. D. Calvert, and E. Whalley, *J. Chem. Phys.*, 1963, **38**, 840.
14 S. Klotz, J. M. Besson, G. Hamel, R. J. Nelmes, J. S. Loveday, and W. G. Marshall, *Nature*, 1999, **398**, 681.
15 D. D. Klug, Y. P. Handa, J. S. Tse, and E. Whalley, *J. Chem. Phys.*, 1989, **90**, 2390.
16 M. Blackman and N. D. Lisgarten, *Adv. Phys.*, 1958, **7**, 189.
17 D. C. Steytler, J. C. Dore, and C. J. Wright, *J. Phys. Chem.*, 1983, **87**, 2458.
18 B. J. Murray and A. K. Bertram, *Phys. Chem. Chem. Phys.*, 2006, **8**, 186.
19 B. J. Murray, D. A. Knopf, and A. K. Bertram, *Nature*, 2005, **434**, 202.
20 T. Kobayashi, Y. Furukawa, T. Takahashi, and H. Uyeda, *J. Cryst. Growth*, 1976, **35**, 262.
21 E. Whalley, *J. Phys. Chem.*, 1983, **87**, 4174.
22 P. Gassendi, 'Phenomenum rarum Romae observatum 20 martij, et ejus causarum explicatio', Amstelodami. Henr. Guerard, 1629.
23 M. Riikonen, M. Sillanpää, L. Virta, D. Sullivan, J. Moilanen, and I. Luukkonen, *Appl. Opt.*, 2000, **39**, 6080.
24 D. M. Murphy, *Geophys. Res. Lett.*, 2003, **30**, 2230.
25 W. F. Kuhs, G. Genov, D. K. Staykova, and T. Hansen, *Phys. Chem. Chem. Phys.*, 2004, **6**, 4917.
26 K. Morishige and H. Uematsu, *J. Chem. Phys.*, 2005, **122**, 044711.
27 D. A. Huckaby, R. Pitis, R. H. Kincaid, and C. Hamilton, *J. Chem. Phys.*, 1993, **98**, 8105.
28 H. Tanaka and I. Okabe, *Chem. Phys. Lett.*, 1996, **259**, 593.
29 M. S. Paterson, *J. Appl. Phys.*, 1952, **23**, 805.
30 Z. Weiss and P. Capkova, *IUCr Monographs on Crystallography*, 1999, **10**, 318.
31 P. Convert, T. Hansen, A. Oed, and J. Torregrossa, *Physica B*, 1998, **241-243**, 195.
32 T. C. Hansen, *Mater. Sci. Forum*, 2004, **443-444**, 181.
33 L. S. Ramsdell, *Am. Mineral.*, 1947, **32**, 64.
34 H. Jagodzinski, *Acta Cryst.*, 1949, **2**, 208.
35 R. Berliner and S. A. Werner, *Phys. Rev. B: Condens. Matter*, 1986, **34**, 3586.
36 Igor Pro 5.04B, Wavemetrics Inc., Lake Oswego, Oregon, USA, 2005.
37 J. Rodriguez-Carvajal, *Physica B*, 1993, **192**, 55.
38 K. Röttger, A. Endriss, J. Ihringer, S. Doyle, and W. F. Kuhs, *Acta Crystallogr., Sect. B: Struct. Sci.*, 1994, **50**, 644.
39 J. Dore, *Chem. Phys.*, 2000, **258**, 327.
40 M. M. Koza, F. Czeschka, H. Schober, T. Hansen, B. Geil, K. Winkel, C. Köhler, and M. Scheuermann, *Phys. Rev. Lett.*, 2005, **94**, 1.